ChemComm

Accepted Manuscript

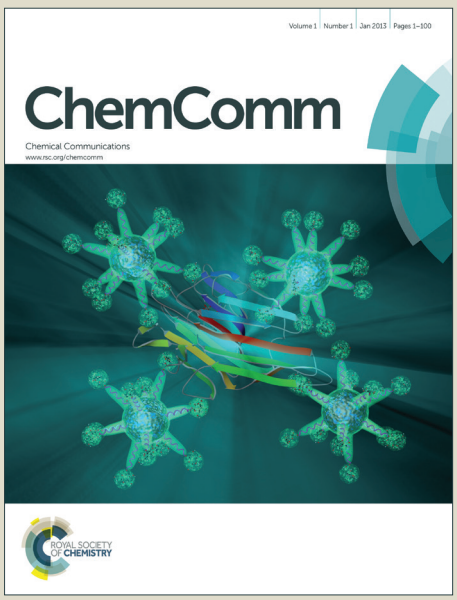

ROYAL SOCIETY OF CHEMISTRY

www.rsc.org/chemcomm

Journal Name

RSCPublishing

COMMUNICATION

Facile One-Pot Synthesis of Multi-Yolk-Shell Bi@C Nanostructures by the Nanoscale Kirkendall Effect

Cite this: DOI: 10.1039/xoxxoooooox

C. M. Cui,[a] X. H. Guo,[a*] Y. M. Geng[a], T. T. Dang,[a] G. Xie,[a*] S. P. Chen,[a] and F. Q. Zhao[b]

Received ooth January 2015,
Accepted ooth January 2015

DOI: 10.1039/xoxxoooooox

www.rsc.org/

A kind of multi-yolk-shell Bi@C nanostructures was prepared via a facile one-pot template-free hydrothermal approach. The prepared Bi@C nanostructures can act as solid catalyst on thermal decomposition of cyclotrimethylenetrinitramine (RDX) and display excellent catalytic activity, which highlight their application in the field of energetic materials.

Recently, synthesis of novel yolk-shell or rattle-type hollow nanostructures has attracted significant attention in many fields. These specific nanostructures have potential applications in catalysis,[1] energy storage,[2,3] drug delivery,[4] gas sensing,[5] and biomedicine.[6] Particularly, newly emerged metal@carbon yolk-shell structures have triggered great attention[7] due to their low density, high surface area, large pore volume, good mechanical stability, and surface permeability. The outer carbon shell usually functions as a barrier to prevent the encapsulated metal nanoparticles from aggregating or coalescing under harsh reaction conditions.[7] For the these metal@carbon hollow nanostructures, the types of carbon precursor can play a vital role in preparation of the metal@carbon hollow framework.[8]

Various methodologies have been developed for the preparation of metal@carbon yolk-shell nanostructures, such as template-assisted methods, emulsion or interfacial polymerization processing, and surface living polymerization reactions.[9] However; most of these approaches generally require complicated procedures, high cost, and relatively harsh conditions, which would limit scalable production and further application. Recently developed template-free methods based on the nanoscale Kirkendall effect,[10] Ostwald ripening,[11] galvanic replacement,[12] and surface-protected etching[13] have shown great potential for engineering hollow nanostructures. These strategies are particularly attractive because the hollow shells are produced via spontaneous chemical reaction without using templates during the hollowing process. The Kirkendall effect can be described as the displacement of the interface between two different solid phases due to unbalanced interdiffusion fluxes from one side of the interface to another.[10f] It usually induces the formation of vacancies within the fast diffusing material. A method based on the nanoscale Kirkendall effect has been successfully applied for synthesizing various hollow metal oxides, chalcogenides, phosphides, nitrides, metals and alloys, and core/shell structures.[10g] However, to our knowledge, there has been limited success in fabricating novel metal@carbon multi-yolk-shell nanostructures via the specific nanoscale Kirkendall effect.

Herein, uniform Bi@C multi-yolk-shell nanostructures are prepared via a facile one-pot template-free hydrothermal approach with the assistance of the specific nanoscale Kirkendall effect. The prepared Bi@C nanostructures serve as solid catalyst on thermal decomposition of cyclotrimethylenetrinitramine (RDX). Moreover, cyclotrimethylenetrinitramine, as a representative ingredient of solid propellants and powerful explosives, is used as a common oxidizer in the rocket propellant. The improvement of the thermolytic and detonation performances of RDX has recently become a popular topic. Currently, the addition of nano metal powder or high-energy additives to improve the thermolysis property of RDX,[14] however, this always bring some disadvantages such as environmental pollution, harsh reaction condition and poor efficiency, and therefore limiting its potential application. As a result, it is of great significance to develop novel catalysts toward decreasing the exothermic decomposition temperature and improving decomposition efficiency of RDX at lower burning temperature.

A black product can be formed after hydrothermal reactions at 200 ^{o}C for 1 h. The prepared sample was subjected to X-ray diffusion (XRD) testing, as shown in Figure 1a. The strong diffraction peaks can be easily indexed as rhombohedra Bi (JCPDS card no. 44-1246), and the obtained Bi species displays good crystalline nature. In addition, no other impurity peaks can be detected, implying that the reduction of Bi^{3+} is complete under the current synthetic conditions. The morphology and microstructure of the synthesized samples were investigated by scanning electron microscope (SEM) and transmission electron microscope (TEM) observations. The prepared sample exhibits well-dispersed yolk-shell morphology with a mean diameter of ~ 600 nm (Figure 1b). In addition, TEM images unambiguously confirm the presence of the typical multi-yolk-shell structure (Figure 1c), in which multiple monodispersed Bi nanoparticles with a size of less than 100 nm are studded into the inner vacancy of the hollow shell layer. The average thickness of the shell layer is about 80 nm, and it displays a well-defined porous structure (Figure 1d). The energy dispersive spectroscopy (EDS) and Raman spectroscopy results further confirm the only presence of C and Bi species in the sample, indicating the

formation of multi-yolk-shell Bi@C nanostructures (Figure 1e and Figure S1). We also investigated the effect of various amounts of glucose on the morphology of the resulting samples; results are shown in supporting information Figure S2.

To study the formation process of the multi-yolk-shell structure, we need to explore the reaction time and reagent concentrations-dependent experiments, respectively. Figure 2 shows TEM images of the prepared products at different reaction times. Before arriving at 200 ^{o}C, glucose underwent decomposition and further carbonation into reductive carbonaceous particles rich in functional groups, such as hydroxyl and carbonyl groups. The Fourier Transform infrared spectroscopy (FTIR) result demonstrates the existence of the groups above, which are located at 3411 and 1653 cm-1 for -OH and -C=O, respectively (Figure S3). Then, a class of network-like aggregate structure can be formed (Figure 2a). On account of the strong oxygen affinity of Bi^{3+}, dissociative Bi^{3+} in hot solution rapidly was coordinated with the functionalized carbonaceous particles and grew into a very tiny transition stated complex (TSC) with size ranging from 5 to 10 nm. Then, a class of core-shell structure consisting of a TSC core and a carbon shell was formed after 4 min (Figure 2b).

Subsequently, the tiny grains are gathered and assembled into large TSC spherical precursors with a diameter of ~200 nm, which is clearly depicted in Figure 2b. With greater reaction time, the formed TSC intermediate suffers from more surface coarseness (Figure 2c). Bi^{3+} ions on the surface of the globular TSC bulk were preferentially reduced into zero-valent Bi by carbonyl groups of glucose, and the separated carbonaceous particles aggregated and cross linked into a thin porous carbon shell to cover the whole TSC bulk. Thus, the diffusion of TSC and carbonaceous particles took place along opposite direction at the surface of TSC and carbon shell (Figure 2d). This phenomenon could be ascribed to the difference of the interdiffusion rates between the carbonaceous particles and TSC intermediate based on the Kirkendall effect.[10c] The Kirkendall effect can give rise to void formation near the bond interface and within the fast-diffusion side, thus deteriorating the bonding strength of the interface.[15] In our study, TSC bulk was enclosed by the carbon layer and voids can be formed at the interface of TSC core and carbon shell at early reaction stage. Hence, we can conclude that the outward diffusion of TSC particles is much faster than the inward diffusion of the carbonaceous particles. Because the outward diffusion of TSC particles is much faster than the inward diffusion of the carbonaceous particles, an inward flux of vacancies would leads to the formation of interior voids at the TSC core/carbon shell interface. With the TSC core being gradually consumed and following this unbalanced diffusion mode from its outer boundary to the inner centre, the carbon shell becomes thicker.

Additionally, due to the outward diffusion of bismuth species being much slower than that of the carbonaceous particles, metallic Bi seeds suspend and migrate randomly inside the carbon shell. Consequently, the concentration of Bi particles grows larger with more reaction time under the thermally activated conditions. Once exceeding supersaturation, these Bi grains immediately undergo nucleation and agglomeration due to the minimization of surface free energy as the reaction proceeds. As a consequence, crystalline Bi particles of about 80 nm are formed due to the steric hindrance and size effect, and they migrate onto the inner surface of the carbon shell (Figure 2e). When the TSC core is consumed, the porous carbon layer stops growing and eventually reaches a shell thickness of ~100 nm. On the other hand, some Bi nanoparticles with the same diameter were formed in the centre of the cavity after reaction for 60 min. A unique class of multi-yolk-shell Bi@C nanostructures with a total diameter of ~600 nm can take shape, in which multiple spherical Bi cores are encapsulated by a carbon shell (Figure 2f). SEM and XRD data further verify these results (supporting information Figures S4 and S5). By comparing the phase compositions of products at different stages, it can be clearly seen that strong diffraction peaks of rhombohedra Bi occur only after 45 min (Figure 4). Based on these results, a schematic illustration depicting the formation of Bi@C multi-yolk-shell structures is presented in Scheme 1.

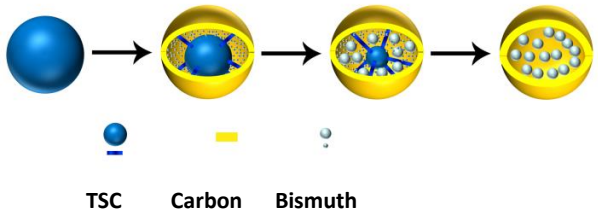

Scheme 1: Schematic illustration of the formation of multi-yolk-shell Bi@C nanostructure by the nanoscale Kirkendall effect

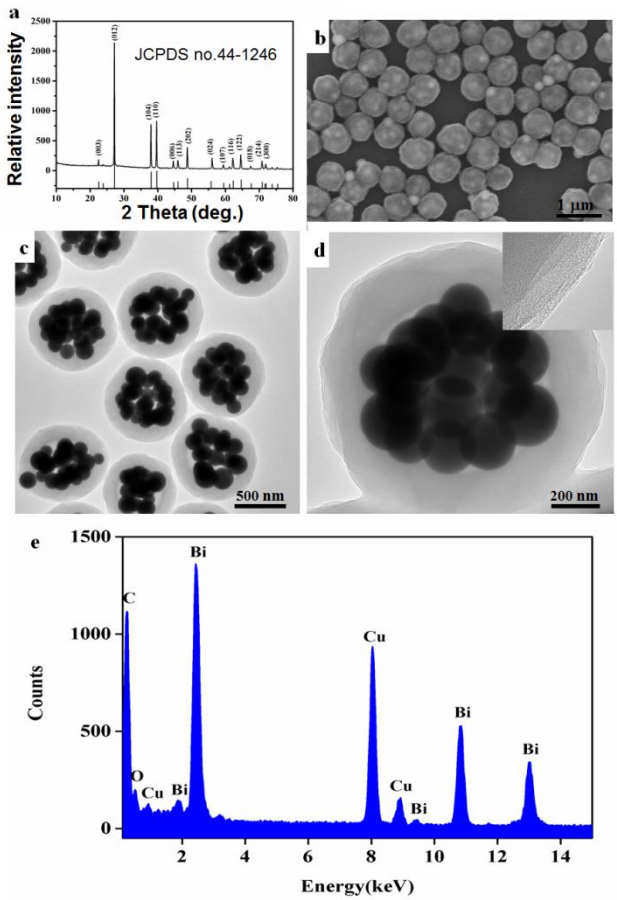

Figure 1. Structure, Morphology and Component analysis for the prepared Bi@C multi-yolk-shell nanostructure, (a) XRD pattern; (b) SEM image; (c, d) TEM images with different magnifications; (e) EDS pattern, the sample was formed in the presence of 0.6 g of glucose via 200 ^{o}C hydrothermal reaction for 1 h.

In order to explore whether the nanoscale Kirkendall effect is applicable to other metal combinations, we have performed some comparative experiments by changing metal salt types, other reaction conditions were constant. Wherein, we choose $Co(NO_3)_2$ and $SnCl_2$ as metal precursors, respectively, then, a hierarchical flower-like C/Co_3O_4 core-shell structure can be fabricated when

$Co(NO_3)_2$ was used as metal precursor, results were shown in Figure S6. In addition, a novel hollow C/SnO_2 nanocomposite was prepared when using $SnCl_2$ as metal precursor, in which many near-cubic SnO_2 particles spreading all over the carbon framework, as shown in Figure S7.

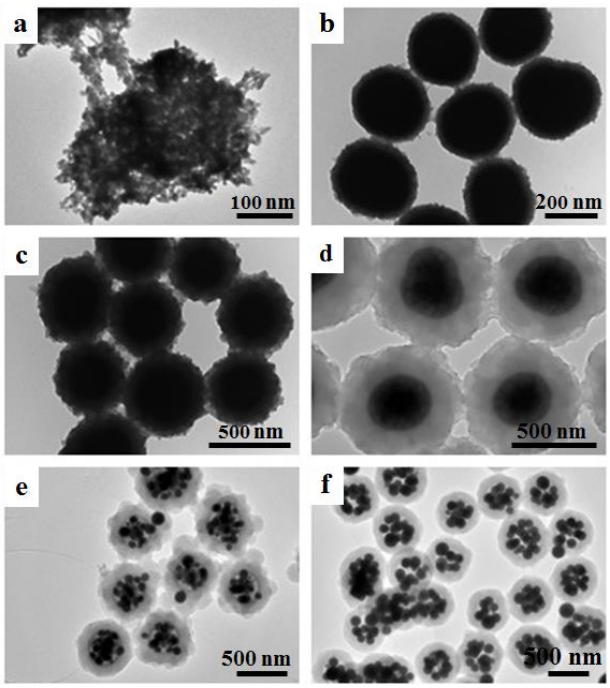

Figure 2. TEM images of Bi@C multi-yolk-shell structural samples synthesized via 200 °C hydrothermal reaction for (a) 0; (b) 4; (c) 15; (d) 30; (e) 45; and (f) 60 min, respectively. Other reaction parameters are kept constant.

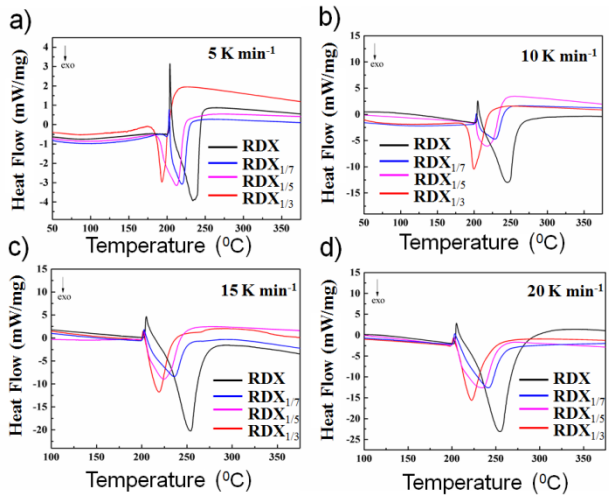

Figure 3. DSC curves of catalytic thermal decomposition of RDX in the presence of different contents of Bi@C at various heating rates under nitrogen atmosphere, wherein, the numbers such as 1/7, 1/5 and 1/3 present the mass ratios of RDX and Bi@C, respectively.

The catalytic activities of the multi-yolk-shell Bi@C structures were evaluated via thermal decomposition of RDX by differential scanning calorimetry (DSC) testing. The decomposition temperature of RDX is basically constant. The decomposition peaks of RDX can be well observed in the DSC curves (Figure 3). Wherein, it was found that sharp exothermic peaks are appeared at different heating rates and mass ratios of RDX and Bi@C, which was ascribed to the sublimation and the melting process of RDX. When the mass ratios of RDX and Bi@C are kept constant, then the typical endothermal peaks display obvious right-shift with the increase of heating rates. Additionally, a broad exothermal peak temperature is 234.1 °C in the absence of Bi@C catalyst at heating rate of 20 K min^{-1}(black line in Figure 3d). However, after mixing Bi@C with RDX, the exothermic peak temperature (Tp) in the presence of Bi@C can be shifted from 234.1 to 192.24 °C, namely, the minimum Tp is 192.24 °C in the case of RDX1/3 at a heating rate of ~ 5 K min^{-1}, which is highly lower comparing to that of pure RDX, the result is very superior to previously reported Tp ~ 207.2 and 209.9 °C when using $La_{0.8}Sr_{0.2}MnO_3$ and $KClO_3$ as catalysts, respectively,[16, 17] implying the best catalytic performance of Bi@C in present catalytic system, the detailed DSC results can be seen in Figure 4 and supporting information in Table 2 and 3. In addition, the catalytic activity comparison for the prepared Bi@C samples with different amounts of glucose is shown in Figure S8. All samples show enhanced catalytic activities toward the RDX decomposition compared with the pure RDX.

Noted that the formed yolk-shell Bi@C with 0.6 g of glucose exhibits the optimal catalytic performance in reducing the decomposition temperature of RDX. This is likely due to the unique internal structure and morphology of Bi@C multi-yolk-shell structures. The multiple Bi nanoparticles were decentralized and located randomly inside the carbon shell. The sags, crests, and porous features on the surface of the carbon shell provide a larger specific surface area, leading to an increase of catalytic activity points and further enhancement of the catalytic efficiency of the Bi@C materials.

Moreover, it was found that surface-adsorbed species such as adsorbed oxygen, water molecule and hydroxyl groups are weakly bounded on the sample surface and usually are considered as the origin of the characteristic catalytic activity, this issue can be well demonstrated in previous literatures.[18,19] Additionally, the related results can be seen in Figure S9 and Table 1. Much more containing-oxygen groups can accelerate the decomposition reaction of RDX and further decrease the thermal-decomposition temperatures.[17, 20] In addition, metal Bi particle inside the shell can be converted into Bi_2O_3 (Figure S10) and sequent deliver certain amounts of heat to favour the thermal-decomposition of RDX, porous carbon matrix serve as assistant catalyst can improve the thermal decomposition efficiency of RDX, similar results can be clarified in previous literature.[20] Therefore, we can conclude that the outstanding catalytic performance of the prepared Bi@C composites over the RDX decomposition is closely related to their special structure and composition.

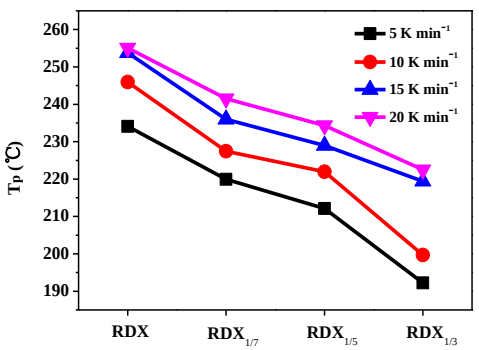

Figure 4: the relationship curves of T_P & the different amounts of RDX mixed with Bi@C catalyst at various heating rates.

Conclusions

In summary, we have demonstrated a facile one-pot hydrothermal synthesis of novel Bi@C multi-yolk-shell nanostructures by the nanoscale Kirkendall effect. It was found that the amounts of glucose are crucial for the thickness control of the carbon shell as well as the number of Bi particles embedded in the final hollow Bi@C structure. The time-dependent experimental results demonstrate that the mechanism involved for the formation of yolk-shell structure was mainly due to the nanoscale Kirkendall effect, which greatly enriches the formation mechanism in the yolk-shell-like multicomponent material systems. RDX catalytic results reveal that the novel yolk-shell Bi@C nanostructures possess outstanding catalytic activity.

Notes and references

[a] Dr. Chengmei Cui, Yanmin Geng, Taotao Dang, Dr. Prof. Xiaohui Guo, Gang Xie, Sanping Chen, Key Lab of Synthetic and Natural Functional Molecule Chemistry of Ministry of Education, and the College of Chemistry and Materials Science, Northwest University, Xi'an 710069, P. R. China. *Corresponding email: guoxh2009@nwu.edu.cn, gxie@nwu.edu.cn

[b] Prof. Fengqi Zhao, Xi'an Modern Chemistry Research Institute, Xi'an 710065, China.

† We acknowledge the funding support from the National Science Foundation of China (NSFC) (No. 21001087, 21173167, 21473135), Program for New Century Excellent Talents in University (NCET-13-0953), the Science and Technology Committee of Shannxi Province (Grant No. 2014KW09-03).

Electronic Supplementary Information (ESI) available: SEM, TEM, XRD patterns, Raman spectrum, XPS, and exothermic decomposition testing data of the prepared samples. See DOI: 10.1039/c000000x/

1 a) S. W. Kim, M. Kim, W. Y. Lee and T. Hyeon, *J. Am. Chem. Soc*. **2002**, 124, 7642; b) Z. Sun, J. Yang, J. Wang, W. Li, S. Kaliaguine, X. Hou, Y. Deng, D. Zhao, *J. Mater. Chem. A*, **2014**, 2, 6071.

2 Y. Wang, M. Wu, Z. Jiao and J. Y. Lee, *Chem. Mater*. **2009**, 21, 3210.

3 Y. Yu, L. Gu, C. B. Zhu, P. A. van Aken and J. Maier, *J. Am. Chem. Soc.* **2009**, 131, 15984.

4 W. R. Zhao, H. R. Chen, Y. S. Li, L. Li, M. D. Lang and J. L. Shi, *Adv. Funct. Mater*. **2008**, 18, 2780.

5 H. Zhang, Q. Zhu, Y. Zhang, Y. Wang, L. Zhao and B. Yu, *Adv. Funct. Mater*. **2007**, 17, 2766.

6 R. Liu, F. L. Qu, Y. L. Guo, N. Yao and R. D. Priestley, *Chem. Commun*. **2014**, 50, 478.

7 a) J. Y. Gong, S. H. Yu, H. S. Qian, L. B. Luo and T. W. Li, *J. Phys. Chem. C*. **2007**, 111, 2490; b) L. J. Zhi, Y. S. Hu, B. EI Hamaoui, X. Wang, I. Lieberwirth, U. Kolb, J. Maier and K. Mullen, *Adv. Mater*. **2008**, 20, 1727; c) Q. Hao, L. Q. Xu, G. D. Li and Y. T. Qian, *Langmuir*. **2009**, 25, 6363; d) T. Yang, J. Liu, Y. Zheng, M. J. Monteiro and S. Z. Qiao, *Chem-Eur. J*. **2013**, 19, 6942; e) S. Ikeda, S. Ishino, T. Harada, N. Okamoto, T. Sakata, H. Mori, S. Kuwabata, T. Torimoto and M. Matsumura. *Angew. Chem. Int. Ed*. **2006**, 45, 7063.

8 a) X. M. Sun and Y. D. Li, *Angew. Chem. Int. Ed*., **2004**, 43, 597; b) W. T. Wang, G. D. Ding, T. Jiang and B. X. Han, *Green. Chem*. **2013**, 15, 1150; c) G. B. Yu, B. Sun, Y. Pei, H. S. Xie, S. R. Yan, M. H. Qiao, K. N. Fan and B. N. Zong, *J. Am. Chem. Soc*. **2010**, 132, 935; d) S. Y. Li, Y. R. Liang, D. C. Wu and R. W Fu, *Carbon*. **2010**, 48, 839; e) N. Baccile, G. Laurent, F. Babonneau, F. Fayon, M. M. Titirici and M. Antonietti, *J. Phys. Chem. C*. **2009**, 113, 9644; f) S. Guo, J. Gong, P. Jiang, M. Wu and S. H. Yu, *Adv. Funct. Mater*, **2008**, 18, 872.

9 a) Q. Wang, H. J. Song, Y. Hu, Y. Su and Y. Lv, *RSC. Advances*. **2014**, 4, 3992; b) T. W. Kimandl and A. Solovyov, *J. Mater. Chem*. **2006**, 16, 1445; c) M. Titirici, A. Thomas and M. Antonietti, *J. Mater. Chem*. **2007**, 17, 3412; d) J. Wang, J. C. Groen, W. B. Yue, W. Z. Zhou and M. O. Coppens, *J. Mater. Chem*. **2008**, 18, 468; e) R. Liu, S. M. Mahurin, C. Li, R. R. Unocic, J. C. Idrobo, H. Gao, S. J. Pennycook and S. Dai, *Angew. Chem. Int. Ed*. **2011**, 50, 6799.

10 a) A. D. Smigelskas and E. O. Kirkendall, *Trans. Am. Inst. Min. Metall. Eng*. **1947**, 171, 130; b) K. Y. Niu, J. Park, H. Zheng and A. P. Alivisatos, *Nano Lett*. **2013**, 13, 5715; c) Y. Ren, W. K. Chim, S. Y. Chiam, J. Q. Huang, C. Pi and J. S. Pan, *Adv. Funct. Mater*. **2010**, 20, 3336; d) Z. J. Yang, I. Lisiecki, M. Walls and M. P. Pileni, *ACS Nano*. **2013**, 7, 1342; e) A. EI Mel, L. Molina-Luna, B. Marie, P. Y. Tessier and K. Du, *ACS Nano*. **2014**, 8, 1854; f) A. Cabot, M. Ibanez, P. Guardia and A. P. Alivisatos, *J. Am. Chem. Soc*. **2009**, 131, 11326; g) W. Wang, M. Dahl and Y. D. Yin, *Chem. Mater*. **2013**, 25, 1179.

11 L. Cao, D. H. Chen and R. A. Caruso, *Angew. Chem. Int. Ed*. **2013**, 52, 10986.

12 M. H. Oh, T. Yu, S. H. Yu, B. Lim, K. T. Ko, M. G. Willinger, D. H. Seo, B. H. Kim, K. Kang, N. Pinna and T. Hyeon, *Science*. **2013**, 340, 964.

13 Y. Zhou, H. R. Chen, L. M. Guo, J. He, F. Chen, J. Zhou, J. W. Feng and J. L. Shi, *ACS Nano*. **2010**, 1, 529.

14 Y. Tong, R. Liu and T. Zhang, *Phys. Chem. Chem. Phys*, **2014**, 16, 17648.

15 Y. Tang, M. Ouyang, *Nat. Mater*, **2007**, 6, 754.

16 Z. X. Wei, L. Gong, Y. Wang and C. W. Hu, *J. Hazardous. Mater*, **2010**, 177, 554.

17 X. F. Dong, Q. L. Yan, X. H. Zhang, D. L. Cao and C. L. Xuan, *J. Anal. Appl. Pyrolysis*, **2012**, 93, 160.

18 M. A. Pe˜na, J. L. G. Fierro, *Chem. Rev*, **2001**, 101, 1981.

19 Z. X. Wei, L. Wei, C. W. Hu, *J. Hazardous. Mater*, **2010**,177, 554.

20 F. Q. Zhao, H. Zhang, T. An, X. H. Zhang, J. H. Yi, S. Y. Xu and Y. L. Wang, *Acta Phys.-Chim. Sin*, **2013**, 29, 777.

